Spin-Polarized STM

Techniques and Applications

Shan Zhong

School of Physics, Peking University

Outline

- Background
- Experimental methods
- Applications

Background

Spin-polarized electron tunneling in planar tunnel junctions

Spin-dependent or spin-polarized tunneling was first observed by Tedrow and Meservey (1971) using planar ferromagnet-oxide-superconductor tunnel junctions.

Background

Spin-polarized electron tunneling in planar ferromagnet-oxide-superconductor tunnel junctions

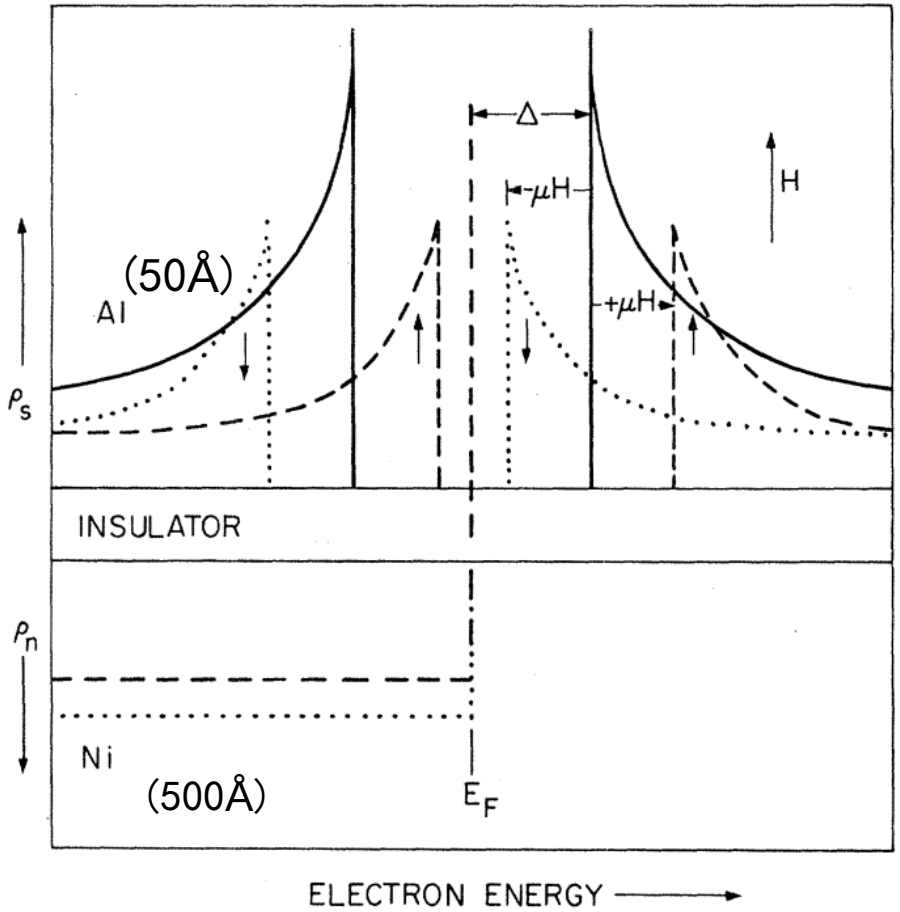

- $Al\text{-}Al_2O_3\text{-}Ni$ junction in strong(up to 50kOe) parallel magnetic field H at 0.4K
- the Zeeman splitting leads to two BCS-type density-of-states curves shifted in energy by $\pm\mu H$

Meservey, R., P. M. Tedrow, and P. Fulde, Phys. Rev. Lett. **25**, 1270–1272

Background

Spin-polarized electron tunneling in planar ferromagnet-oxide-superconductor tunnel junctions

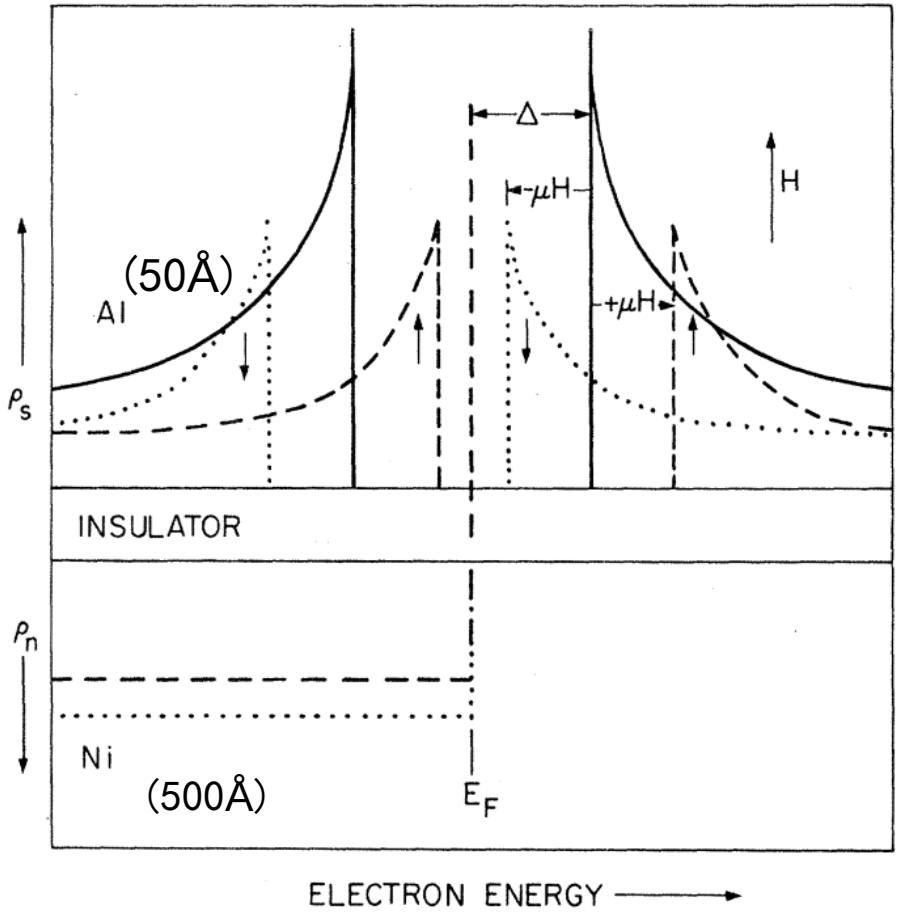

$$\rho_{sc}(E) = \frac{|E|}{\sqrt{(E^2 - \Delta^2)}}, \quad \text{if} |E| \geqslant \Delta,$$

$$\rho_{sc}(E) = 0, \quad \text{if} |E| < \Delta,$$

$$\rho_{sc}(E)_{\uparrow,\downarrow} = \frac{|E|}{\sqrt{(E^2 - \Delta^2)} \mp \mu H}$$

Meservey, R., P. M. Tedrow, and P. Fulde, Phys. Rev. Lett. **25**, 1270–1272

Background
Spin-polarized electron tunneling in planar ferromagnet-oxide-superconductor tunnel junctions

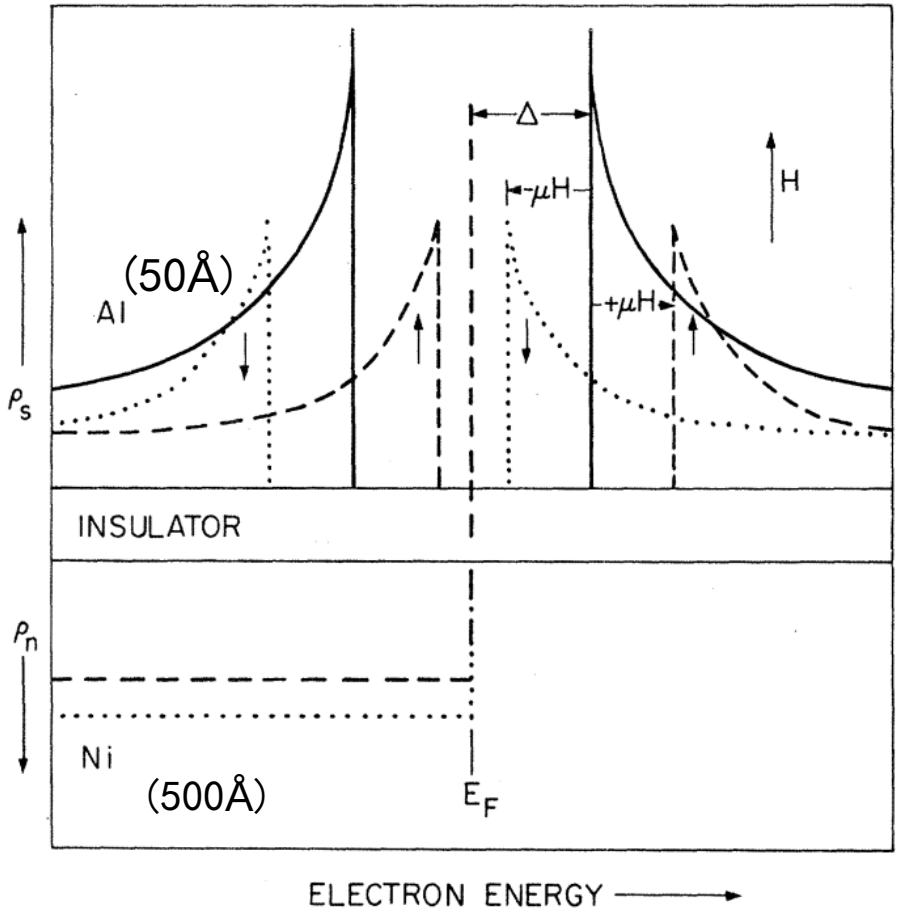

- For the ferromagnetic metal(Ni),spin-down states(dotted) are more numerous than spin-up states(dashed) due to polarization.

Meservey, R., P. M. Tedrow, and P. Fulde, Phys. Rev. Lett. **25**, 1270–1272

Background

Spin-polarized electron tunneling in planar ferromagnet-oxide-superconductor tunnel junctions

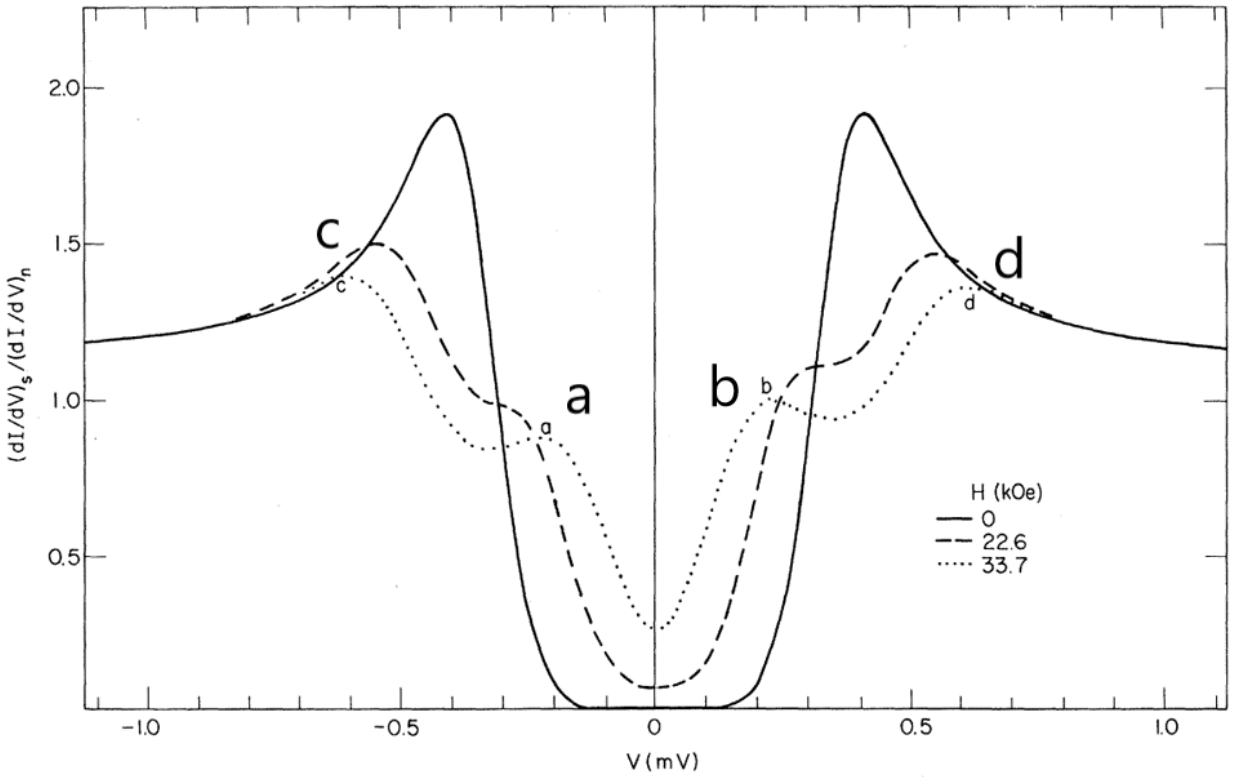

- The asymmetry of conductance peaks a,b,c and d resulting from polarization of Ni
- σ_b/σ_a is a function of polarization

Meservey, R., P. M. Tedrow, and P. Fulde, Phys. Rev. Lett. **25**, 1270–1272

Background

Spin-polarized electron tunneling in planar ferromagnet-oxide-superconductor tunnel junctions

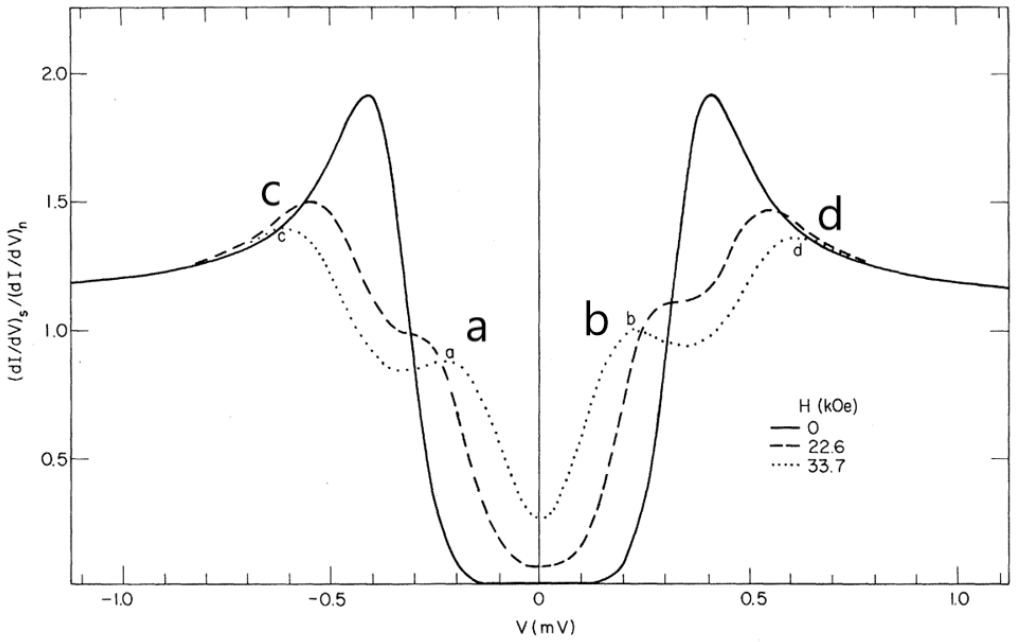

We assume there is no spin-flip during tunneling!

As the Al voltage increases, the Ni FS is displaced to the right, so we expect a peak at b. The corresponding negative voltage peak a is smaller because of the smaller spin-up DOS at the FS assumed for Ni.

Meservey, R., P. M. Tedrow, and P. Fulde, Phys. Rev. Lett. **25**, 1270–1272

Background

Spin-polarized electron tunneling in planar ferromagnet-insulator-ferromagnet tunnel junctions

Also observed by

Julliè re, 1975, Phys. Lett. A 54, 225–226.;

Maekawa and G äfvert, 1982, IEEE Trans. Magn. 18, 707–708.

Spin-resolved scanning tunneling microscopy

The total tunneling conductance G in the limit of small applied bias voltage:

$$G = 2\pi^2 G_0 (n_t^{\uparrow} n_s^{\uparrow} |M_{\uparrow\uparrow}|^2 + n_t^{\uparrow} n_s^{\downarrow} |M_{\uparrow\downarrow}|^2 + n_t^{\downarrow} n_s^{\uparrow} |M_{\downarrow\uparrow}|^2 + n_t^{\downarrow} n_s^{\downarrow} |M_{\downarrow\downarrow}|^2).$$

By introducing

$$n_t = n_t^{\uparrow} + n_t^{\downarrow}, \quad n_s = n_s^{\uparrow} + n_s^{\downarrow} \quad m_t = n_t^{\uparrow} - n_t^{\downarrow}, \quad m_s = n_s^{\uparrow} - n_s^{\downarrow}.$$

And $P_t = m_t / n_t, \quad P_s = m_s / n_s,$

We can obtain $G = 2\pi^2 G_0 |M_0|^2 n_t n_s (1 + P_t P_s \cos\theta).$

Background
Spin-resolved scanning tunneling microscopy

$$G = 2\pi^2 G_0 |M_0|^2 n_t n_s (1 + P_t P_s \cos\theta).$$

- The tunneling conductance in the magnetic case is expected to depend on the spin-resolved local density of states at the Fermi energy for both electrodes and on the cosine of the angle θ between the magnetization directions of tip and sample.
- For the more general case of finite bias voltage, consistent results have been derived.(Wortmann et al. Phys. Rev. Lett. 86, 4132–4135.)

Wiesendanger, R. *Reviews of Modern Physics*, *81*(4), 1495.

Background

Spin-resolved scanning tunneling microscopy

The first experimental observation of vacuum tunneling with spin-polarized electrons based on the use of STM involving a magnetic tip and a magnetic sample was by Wiesendanger, Güntherodt, *et al.(1990)*

The experiment was performed using an UHV STM setup with a Cr(001) sample surface and electrochemically etched ferromagnetic CrO_2 tips.

Background
Spin-resolved scanning tunneling microscopy

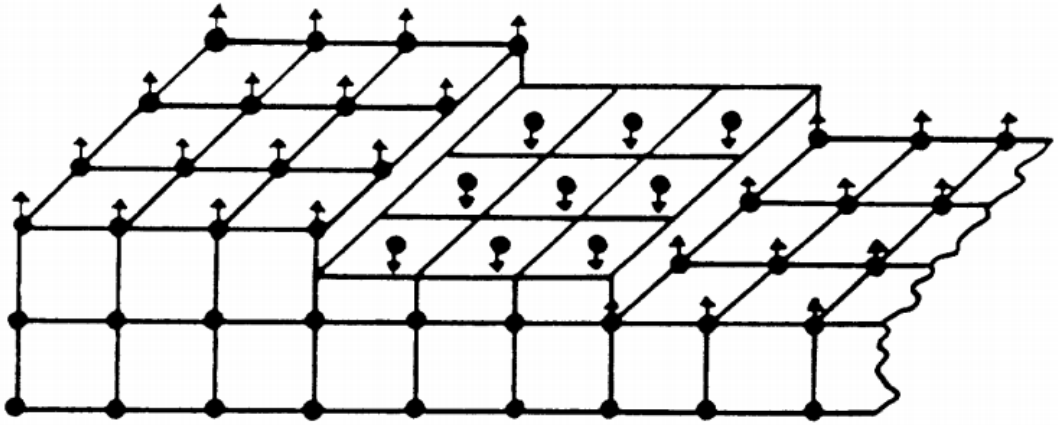

Cr(001)surface

Blugel, Pescia, and Dederichs's calculation predicted topological antiferromagnetism between ferromagnetic terraces separated by single steps.

S. Blugel, D. Pescia, and P. H. Dederichs, Phys. Rev. B 39, 1392 (1989)

Background
Spin-resolved scanning tunneling microscopy

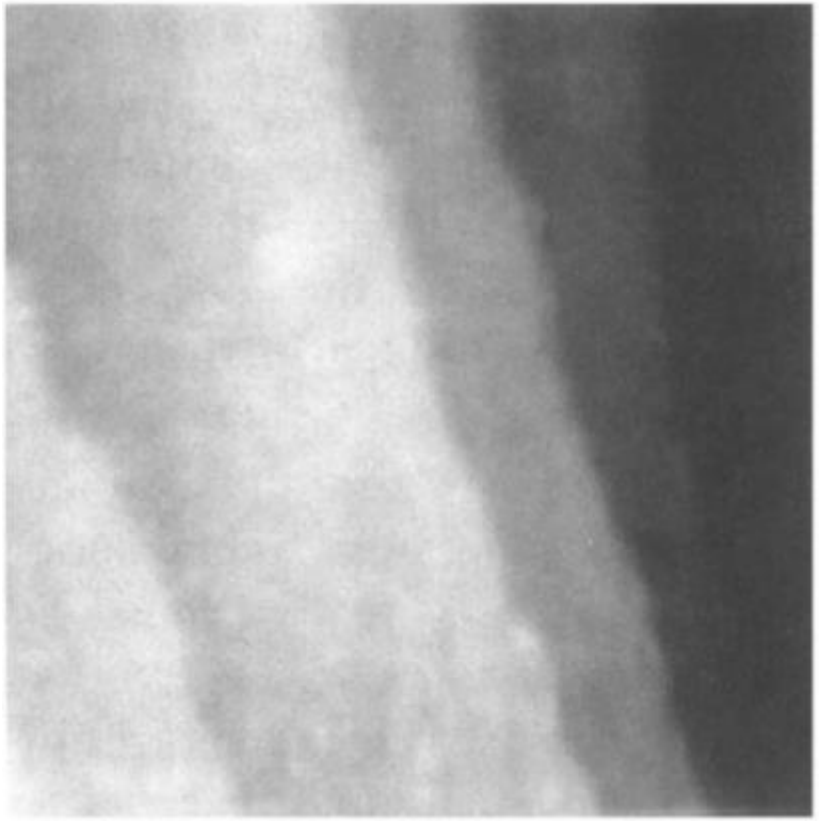

Topographic STM image showed terraces separated by monatomic steps.

Wiesendanger, R., H.-J. Güntherodt, G. Güntherodt, R. J.Gambino, and R. Ruf, Phys. Rev. Lett. **65**, 247–250

Background
Spin-resolved scanning tunneling microscopy

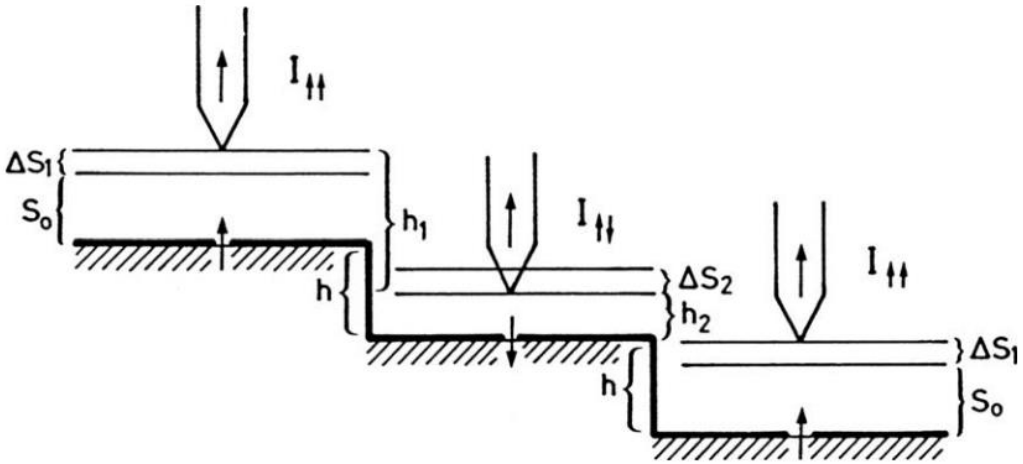

If the magnetic tip were scanned at a constant distance s_0 from the sample surface, the tunneling current would alternate between $I_{\uparrow\uparrow}=I_0(1+P)$ and $I_{\uparrow\downarrow}=I_0(1-P)$, where P denotes the effective polarization of the tunnel junction.

Wiesendanger, R., H.-J. Güntherodt, G. Güntherodt, R. J.Gambino, and R. Ruf, Phys. Rev. Lett. **65**, 247–250

Background
Spin-resolved scanning tunneling microscopy

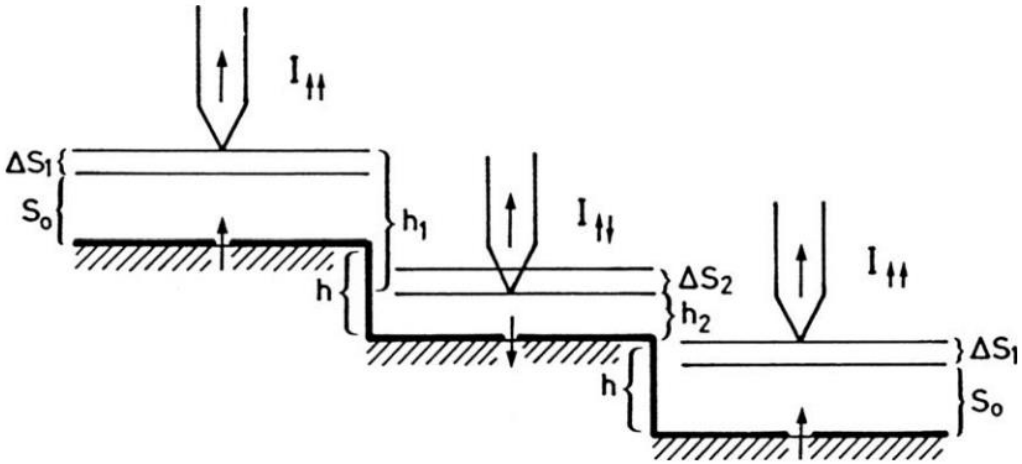

If the SP-STM is performed at a constant current, the feedback system has to adjust the distance of the tip from the sample surface accordingly.

As a consequence, the measured monatomic step heights alternate between $h_1 = h + s_1 + s_2$ and $h_2 = h - s_1 - s_2$

Wiesendanger, R., H.-J. Güntherodt, G. Güntherodt, R. J.Gambino, and R. Ruf, Phys. Rev. Lett. **65**, 247–250

Background
Spin-resolved scanning tunneling microscopy

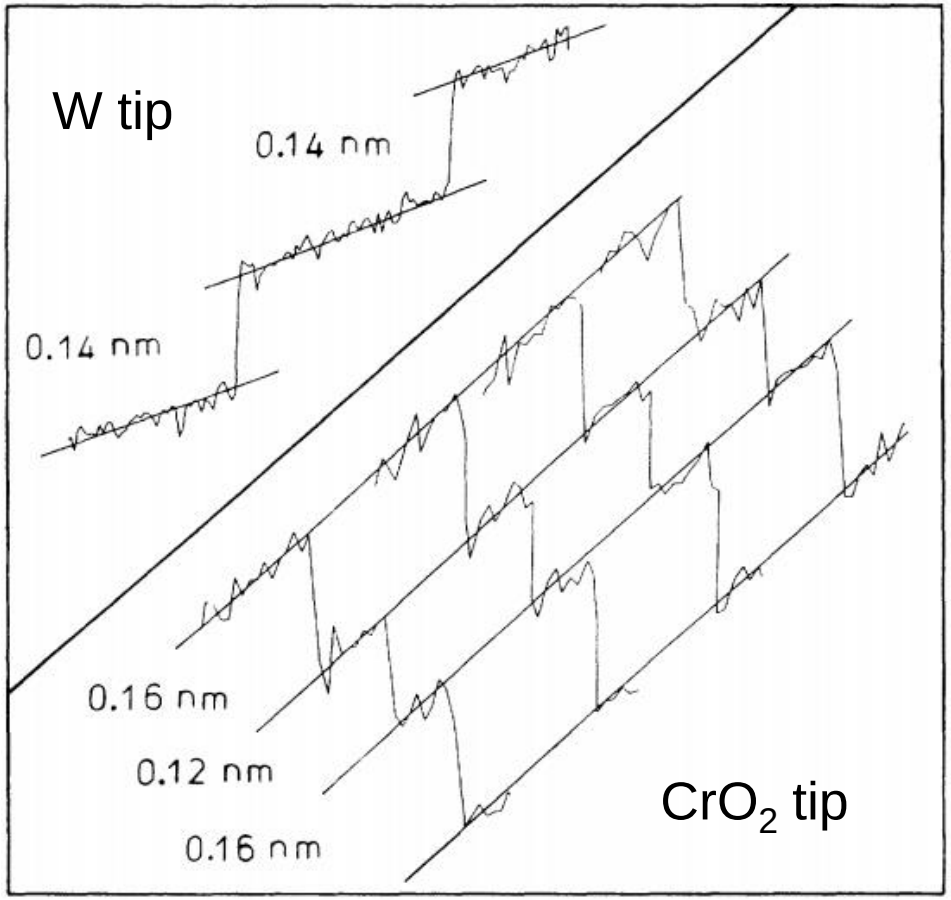

Periodic alternation of the monatomic step-height value is observed.

The inset shows a single-line scan over two monatomic steps obtained with a W tip.

Wiesendanger, R., H.-J. Güntherodt, G. Güntherodt, R. J.Gambino, and R. Ruf, Phys. Rev. Lett. **65**, 247–250

Experimental Methods
spin-sensitive probe tips

Aim:
to prepare suitable probe tips offering simultaneously
a high spatial resolution (down to the atomic level),
a high spin polarization (thereby yielding a high signal-to-noise ratio),
and a nondestructive magnetic imaging process.

Experimental Methods
spin-sensitive probe tips **from bulk magnetic material**

- Made from bulk ferromagnetic 3d transition metal:
- large magnetic stray fields which restrict their application to ferrimagnetic and antiferromagnetic samples, which are nearly insensitive to external magnetic fields

- Made from amorphous alloys with a low saturation magnetization:
- residual magnetic stray field

- Made from antiferromagnetic bulk materials(such as Cr or MnNi) :
- preferable for a nondestructive magnetic imaging process

Wiesendanger, R. *Reviews of Modern Physics*, *81*(4), 1495

Experimental Methods
spin-sensitive probe tips **from bulk magnetic material**

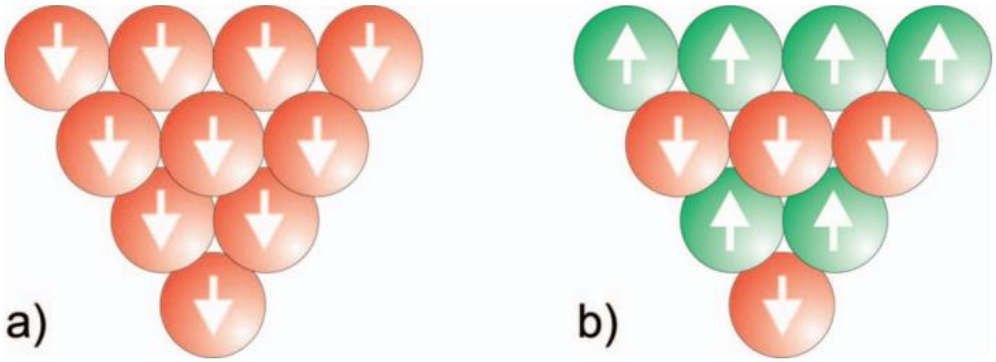

(the apex of a ferromagnetic and an antiferromagnetic tip)

In both cases, the spin state of the front atom determines the spin contrast in SP-STM.

Only in the case of an antiferromagnetic tip can the disturbing influence of long-range magnetic stray fields be avoided.

Wiesendanger, R. *Reviews of Modern Physics*, *81*(4), 1495

Experimental Methods

spin-sensitive probe tips **from bulk magnetic material**

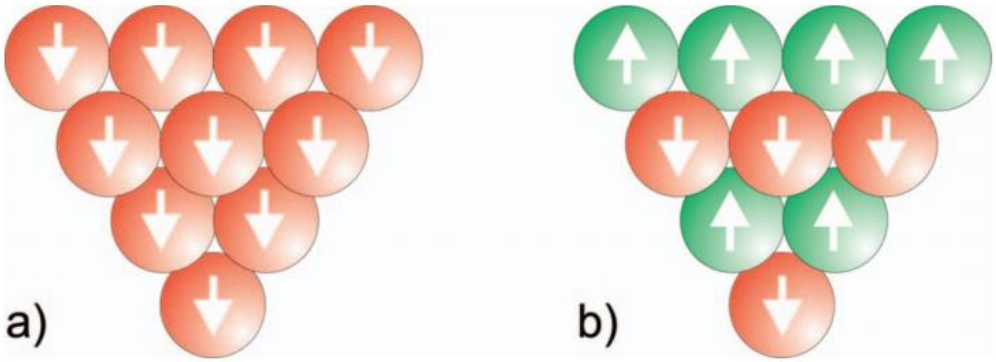

(the apex of a ferromagnetic and an antiferromagnetic tip)

A few uncompensated spins may still exist due to the roughness of a sharp tip, leading to a nonvanishing, but in most cases negligible residual dipolar stray field from AFM tips.

Wiesendanger, R. *Reviews of Modern Physics*, *81*(4), 1495

Experimental Methods
spin-sensitive probe tips **from bulk magnetic material**

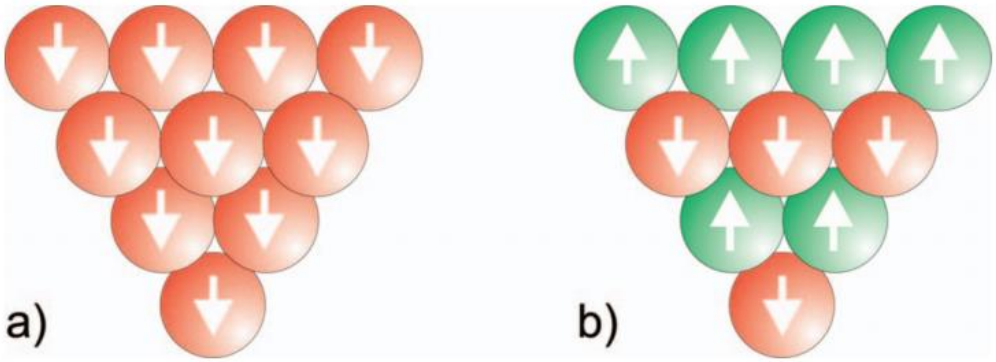

(the apex of a ferromagnetic and an antiferromagnetic tip)

However, blunt AFM probes are not magnetic sensitive because the contributions to the spin-polarized tunneling current from the two different spin sublattices will cancel each other.

Wiesendanger, R. *Reviews of Modern Physics*, *81*(4), 1495

Experimental Methods

spin-sensitive probe tips **from bulk magnetic material**

Also, the spin contrast in SP-STM images has to be sufficiently high, calling for careful choice of materials.

Experimental Methods

spin-sensitive probe tips **from nonmagnetic tips covered with an ultrathin film of magnetic material**

removes oxides and other types of contamination

electrochemical etching of a nonmagnetic tip

in situ cleaning procedure by electron bombardment

A high-temperature flash

thin-film deposition

Experimental Methods

spin-sensitive probe tips **from nonmagnetic tips with a cluster of magnetic material at the front end**

- applying voltage pulses (e.g., 10 V, 60μs)between a standard nonmagnetic STM tip (e.g., W, PtIr)and a magnetic sample
- As a result of the large electric field applied, material can be transferred from the magnetic sample to the tip due to a field desorption process.
- Consequently, a magnetic cluster is obtained.

Yamada, T. K., M. M. J. Bischoff, T. Mizoguchi, and H. van Kempen
Appl. Phys. Lett. **82**, 1437–1439.

Experimental Methods

spin-sensitive probe tips **from nonmagnetic tips with a cluster of magnetic material at the front end**

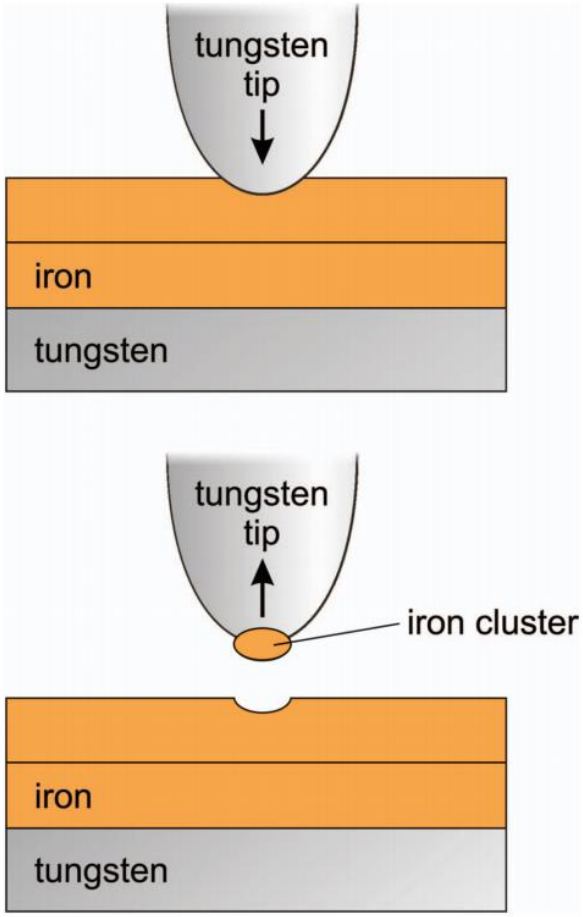

- A nonmagnetic metallic tip might be dipped into a magnetic sample by several nanometers and subsequently retracted.
- If the materials for tip and sample are chosen such that the magnetic sample material **wets** the tip, a stable SP-STM probe can be obtained
- much less demanding

Berbil-Bautista, L., S. Krause, M. Bode, and R. Wiesendanger, Phys.Rev. B **76**, 064411.

Experimental Methods

Possible operation modes of SP-STM: **constant current**

- From earlier discussions, we may assume that the measured tunneling current can be decomposed into spin-averaged and spin-dependent contributions.
- In other words, topographic features and magnetic structures might interfere using constant current mode.
- However, it is shown that ultimate resolution in magnetic imaging can be realized under constant current mode.(Wortmann, et.al.Phys. Rev.Lett. **86**, 4132–4135.)

Experimental Methods

Possible operation modes of SP-STM: **constant current**

$$\Delta I(\vec{r}_{\parallel}, z, U, \theta) = \sum_{n \neq 0} \Delta I_{\vec{q}^{\mathrm{n}}}(z, U, \theta) e^{i\vec{q}^{\mathrm{n}} \cdot \vec{r}},$$

- Since magnetic superstructure leads to larger periodicities in real space compared to a non-magnetic state, the corresponding reciprocal lattice vectors become smaller than those related to the chemical unit cell.
- The expansion coefficients for the spin-polarized contribution to the tunneling current become exponentially larger than those of the non-polarized part.

Wiesendanger, R. *Reviews of Modern Physics*, *81*(4), 1495

Experimental Methods

Possible operation modes of SP-STM: **Spin-resolved spectroscopic mode**

$$\frac{dI}{dU}(R_t,U) \propto n_t n_s(R_t,E_F+eU) + \vec{m}_t \cdot \vec{m}_s(R_t,E_F+eU).$$

The spin-polarized part of the differential tunneling conductance is directly proportional to the spin-polarized LDOS at the energy E_F+eU.

Experimental Methods

Possible operation modes of SP-STM: **Spin-resolved spectroscopic mode**

A separation of the spin-averaged and spin-resolved contributions to the differential tunneling conductance is easy as long as the sample surface exhibits homogeneous electronic properties.

Experimental Methods

Possible operation modes of SP-STM: **Spin-resolved spectroscopic mode**

For sample surfaces with an inhomogeneous electronic structure, a separation of electronic and magnetic structure information can be achieved by comparing two simultaneously recorded *dI*/*dU* images, one obtained with a bias voltage where the spin asymmetry defined by

$$A = \frac{dI/dU_{\uparrow\uparrow} - dI/dU_{\uparrow\downarrow}}{dI/dU_{\uparrow\uparrow} + dI/dU_{\uparrow\downarrow}}$$

becomes zero (electronic contrast image) and a second one obtained with a different bias voltage where the spin asymmetry is maximum (magnetic contrast image).

Experimental Methods

Possible operation modes of SP-STM: **Modulated tip magnetization mode**

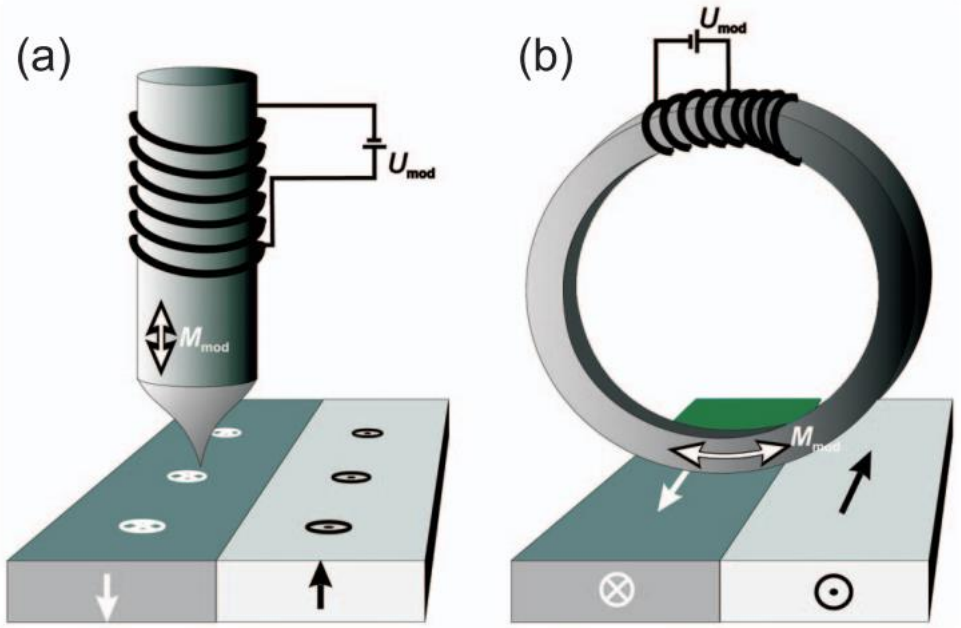

By developing two different kinds of experimental setup, it has become possible to probe both out-of-plane and in-plane components of the sample magnetization.

Experimental Methods

Possible operation modes of SP-STM: **Modulated tip magnetization mode**

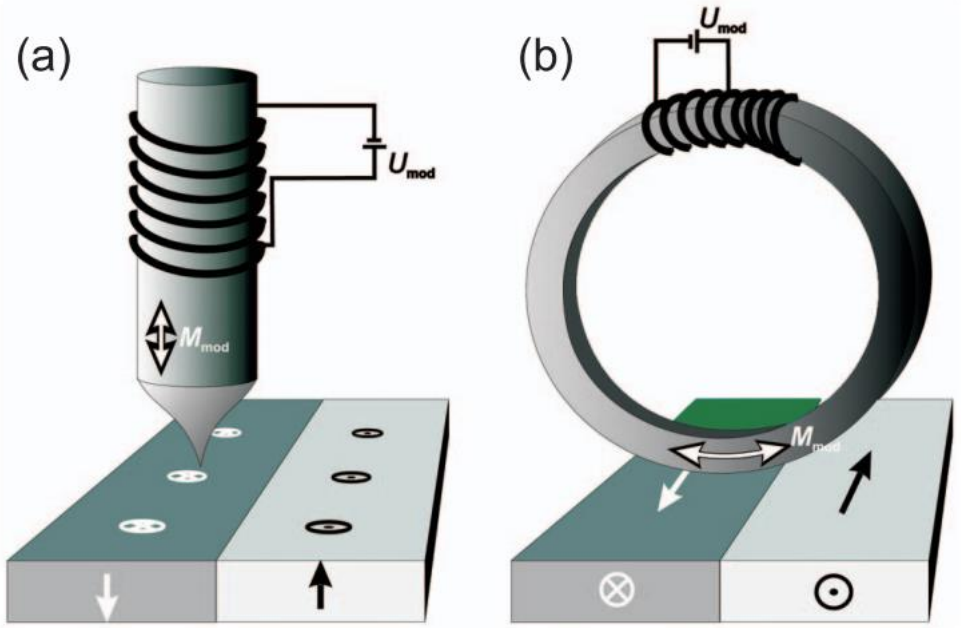

However, this approach suffers from the fact that ferromagnetic probe tips have to be used and their magnetic stray field can affect the local magnetization distribution. Also, this approach is demanding.

Applications

Magnetic domain and domain-wall structure mapping

the determination of magnetic domain and domain-wall structures at a length scale inaccessible by other magnetic imaging techniques

Applications
Magnetic domain and domain-wall structure mapping

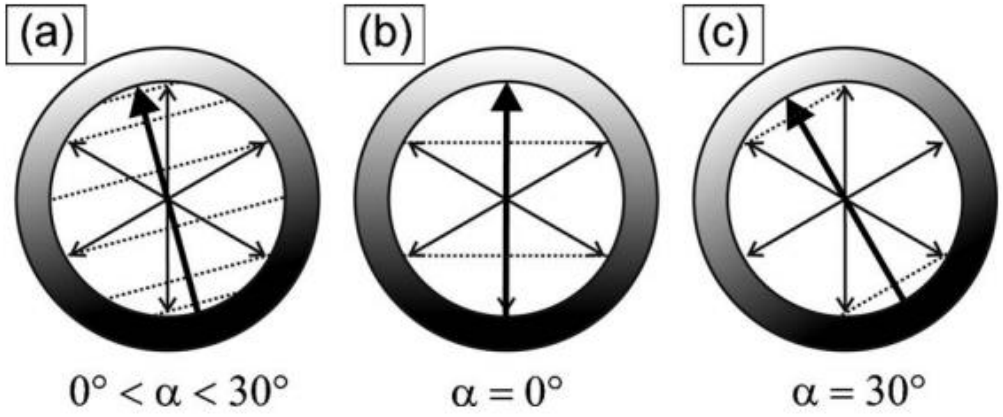

- thin Dy(0001) film (90 ML) grown epitaxially on a W(110) substrate

- Possible orientations of the tip magnetization (thick arrow) with respect to the six possible easy axis magnetization directions of Dy, resulting in six, four, and three contrast levels, respectively.

Berbil-Bautista, L., et al.
Physical Review B 76.6 (2007): 064411.

Applications
Magnetic domain and domain-wall structure mapping

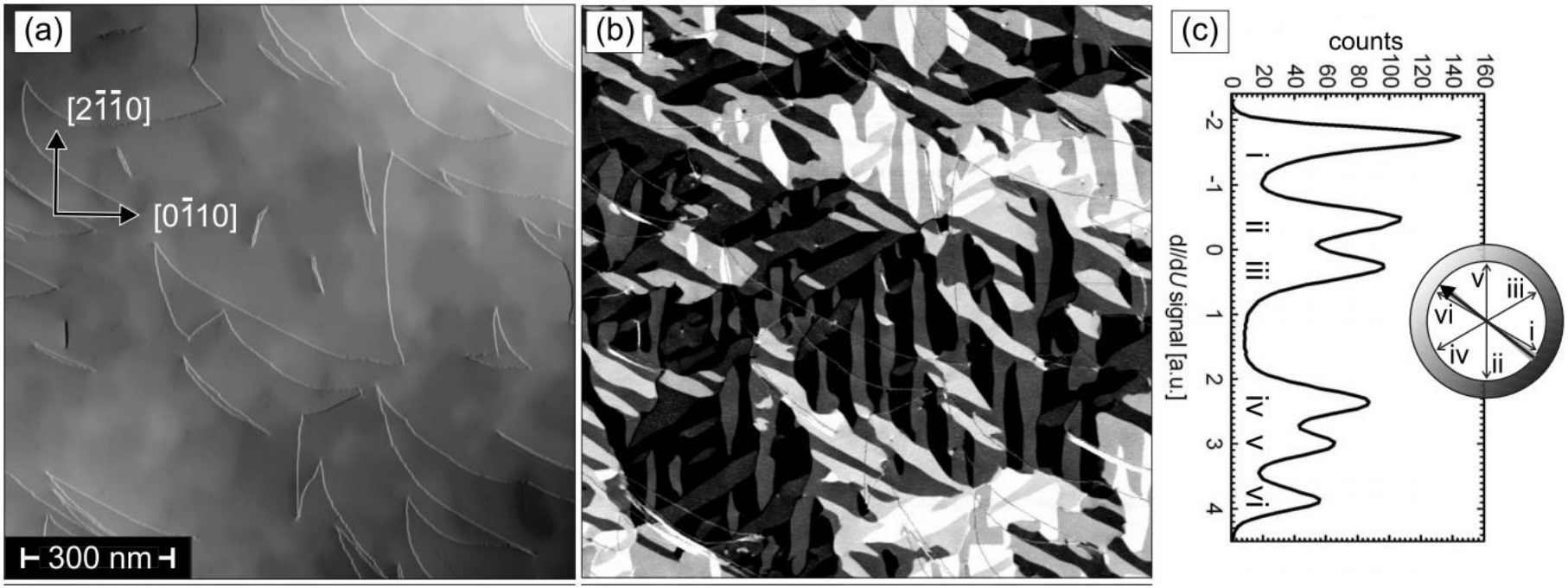

Topography and spin-resolved *dI*/*dU* map of a 90 AL Dy/W(110) film (*T*=25 K, *U*=−1.0 V, and *I*=30 nA).(in-plane sensitive tips)

Berbil-Bautista, L., et al.
Physical Review B 76.6 (2007): 064411.

Applications

Magnetic domain and domain-wall structure mapping

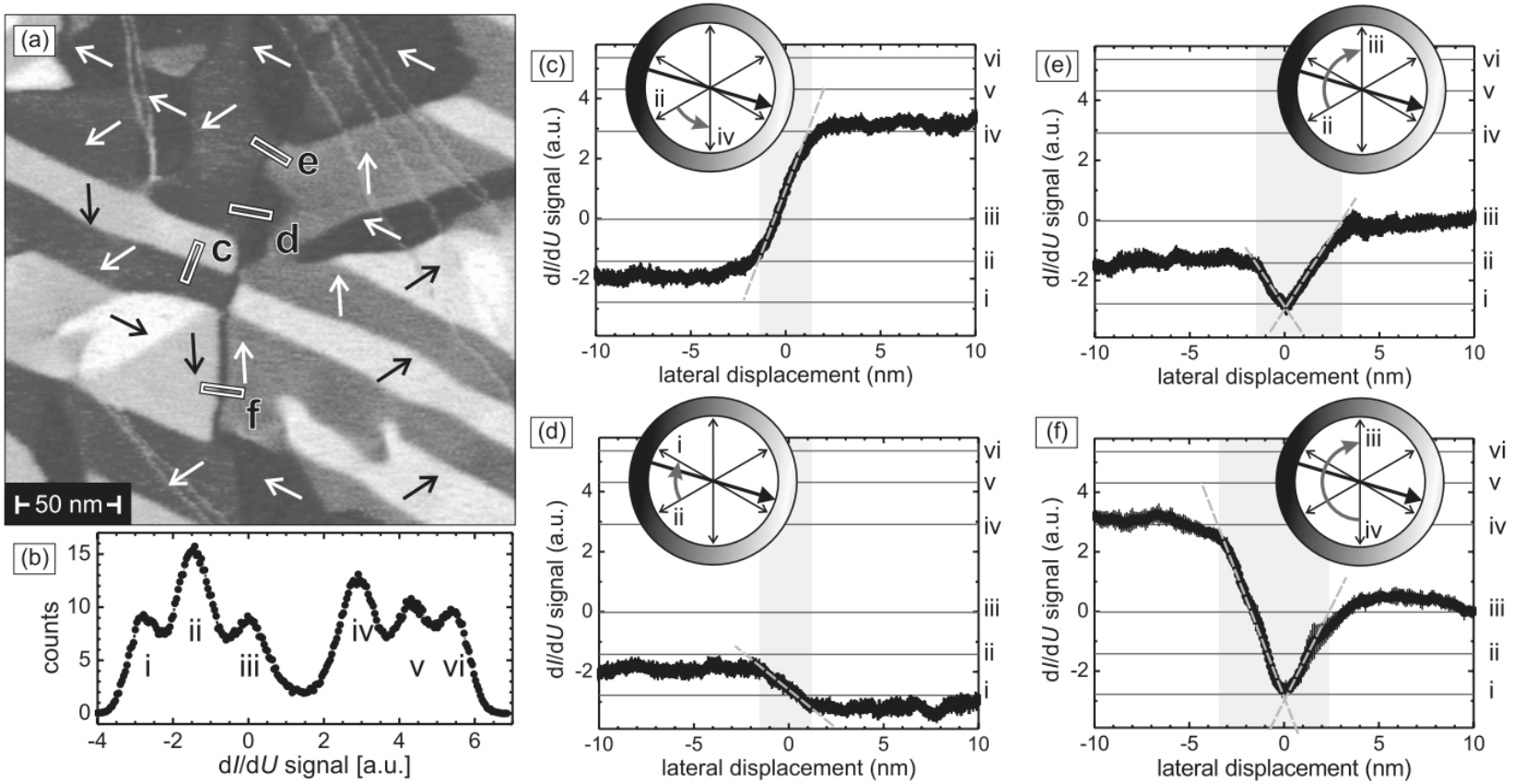

T=59 K, *U*=−0.6 V, and *I*=30 nA

Berbil-Bautista, L., et al.
Physical Review B 76.6 (2007): 064411.

Applications
Magnetic domain and domain-wall structure mapping

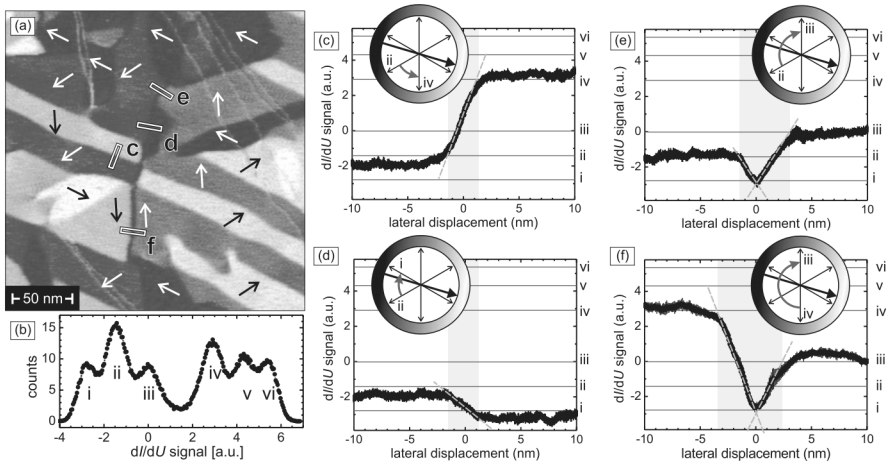

- Domain wall profile analysis of a 90 AL Dy/W film.
- Line profiles and schematic representation of the path of the magnetization for the domain walls.
- The width of the domain walls are identified as about 2-5nm.

Berbil-Bautista, L., et al.
Physical Review B 76.6 (2007): 064411.

Applications

Atomic resolution spin mapping

the very primary motivation of combining the atomic resolution capability of STM and spin sensitivity

Applications
Atomic resolution spin mapping

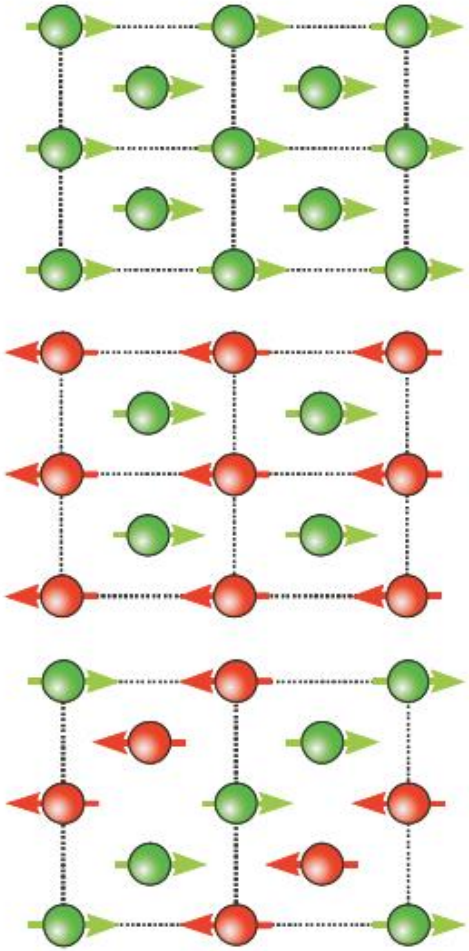

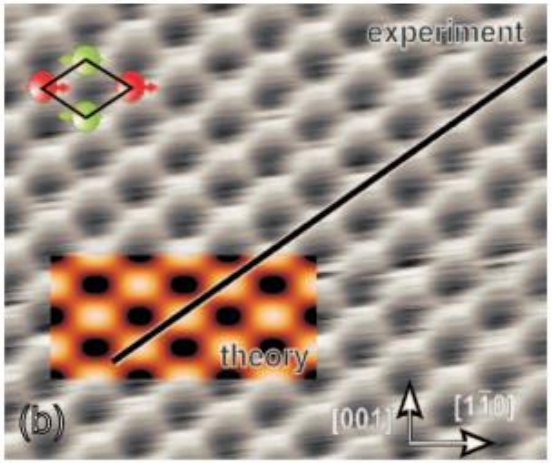

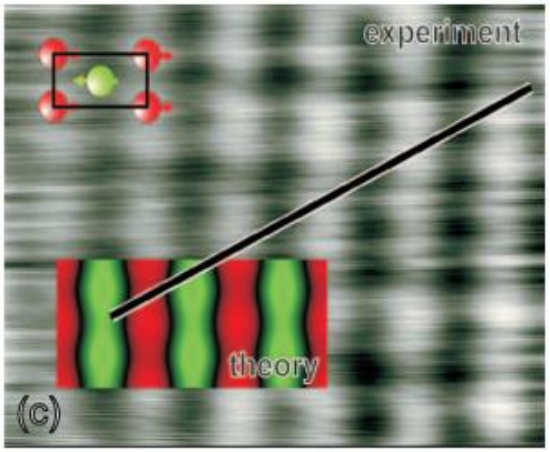

- DFT(spin-polarized LDA) calculations predict magnetic ground state configuration to be c(2x2)-AFM

Heinze, S., et al. *Science* 288.5472 (2000): 1805-1808.

Applications
Atomic resolution spin mapping

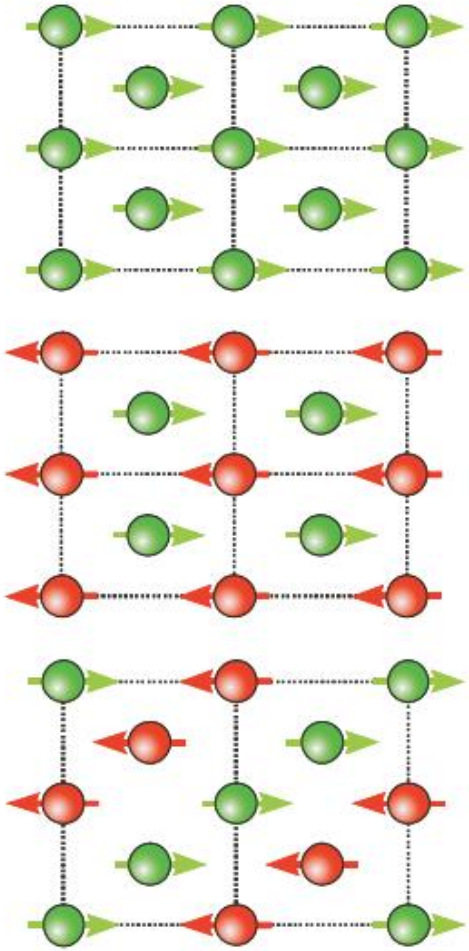

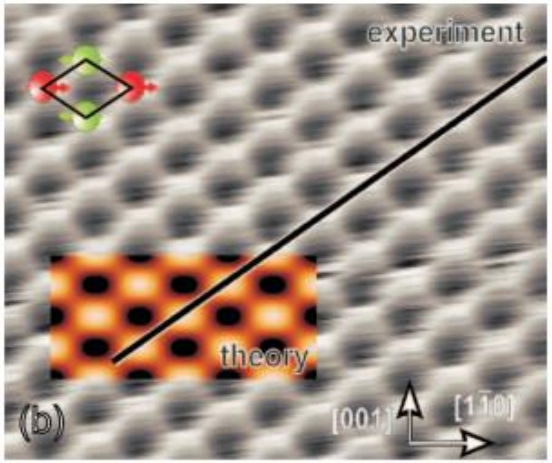

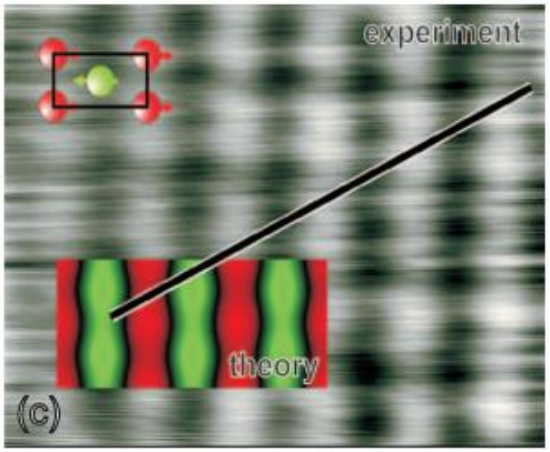

- STM imaging in the constant-current mode of operation performed with a nonmagnetic W tip, and an in-plane sensitive Fe-coated W tip, respectively.

Heinze, S., et al. *Science* 288.5472 (2000): 1805-1808.

Applications
Atomic resolution spin mapping

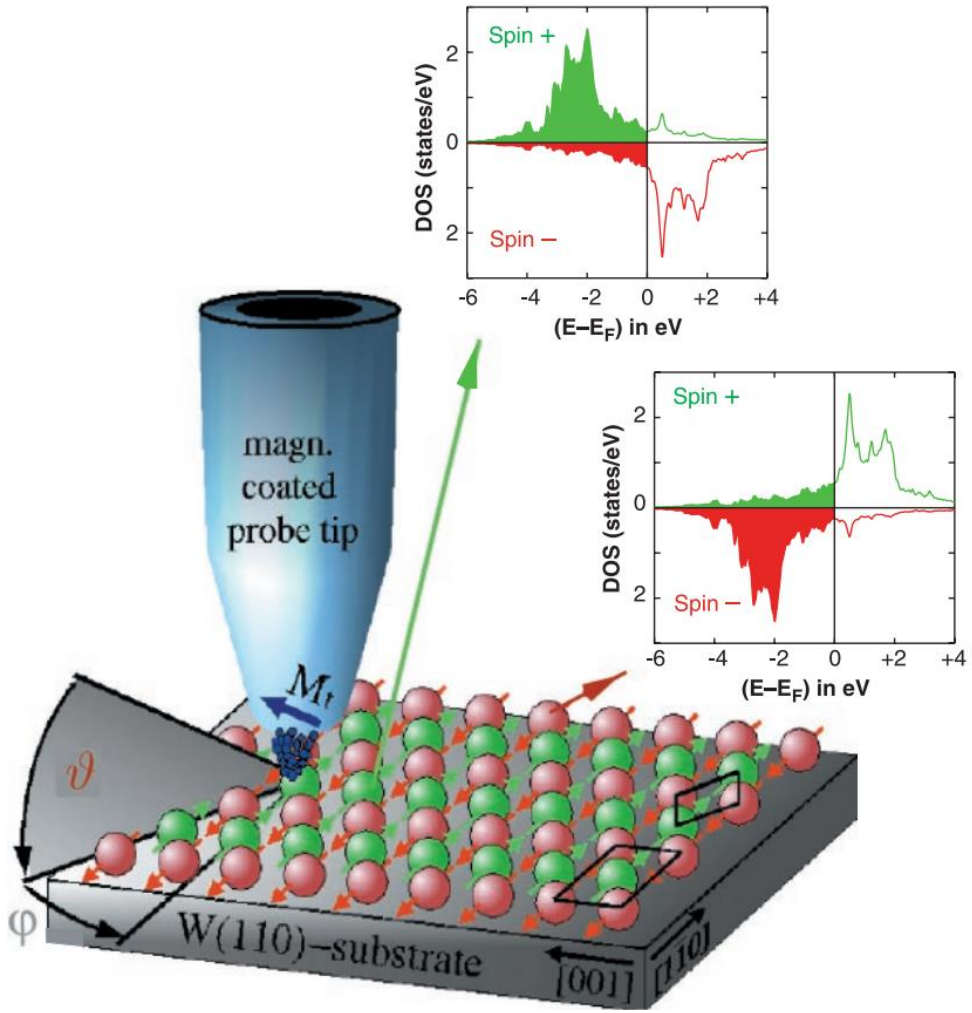

It should be emphasized that SP-STM was the first experimental method capable of showing AFM order in quasi-two-dimensional atomic layers on nonmagnetic substrates.

Heinze, S., et al. *Science* 288.5472 (2000): 1805-1808.

Applications

Spin spiral states as an example of noncollinear spin structure

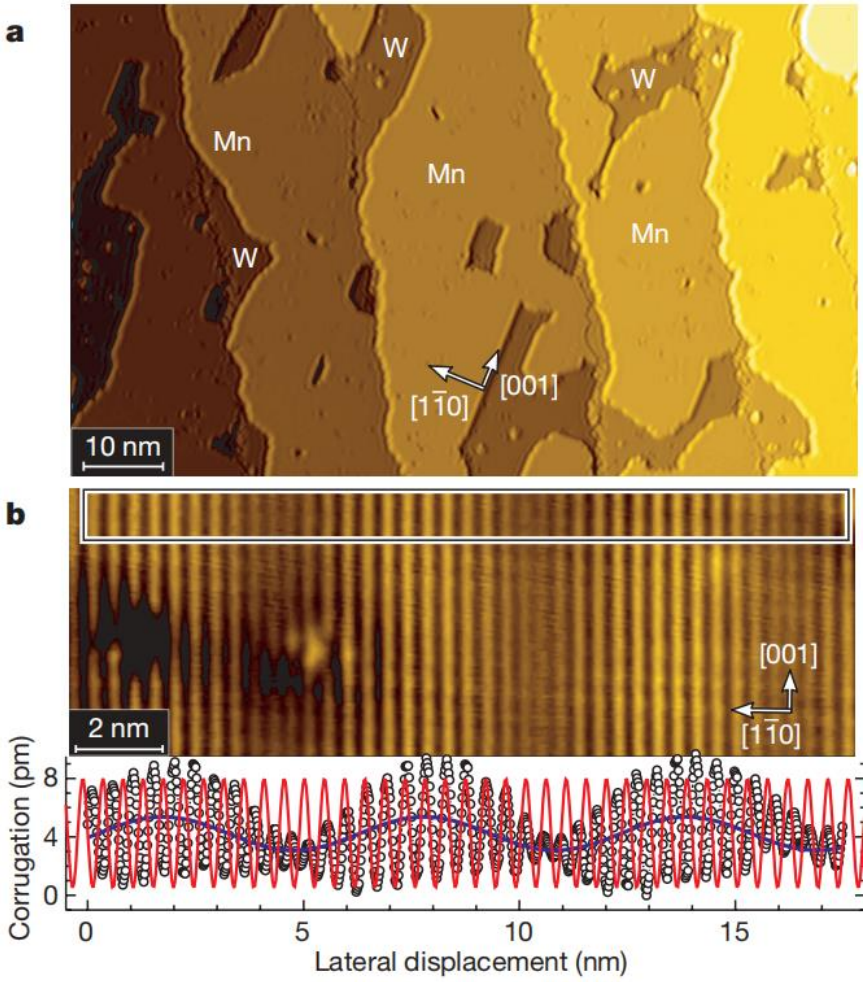

- a single atomic layer of Mn pseudomorphically grown on a W(110) substrate
- Periodic stripes running along the[001] direction, with an inter-stripe distance of about 0.47nm matching the surface lattice constant

Bode, Matthias, et al.
Nature 447.7141 (2007): 190

Applications

Spin spiral states as an example of noncollinear spin structure

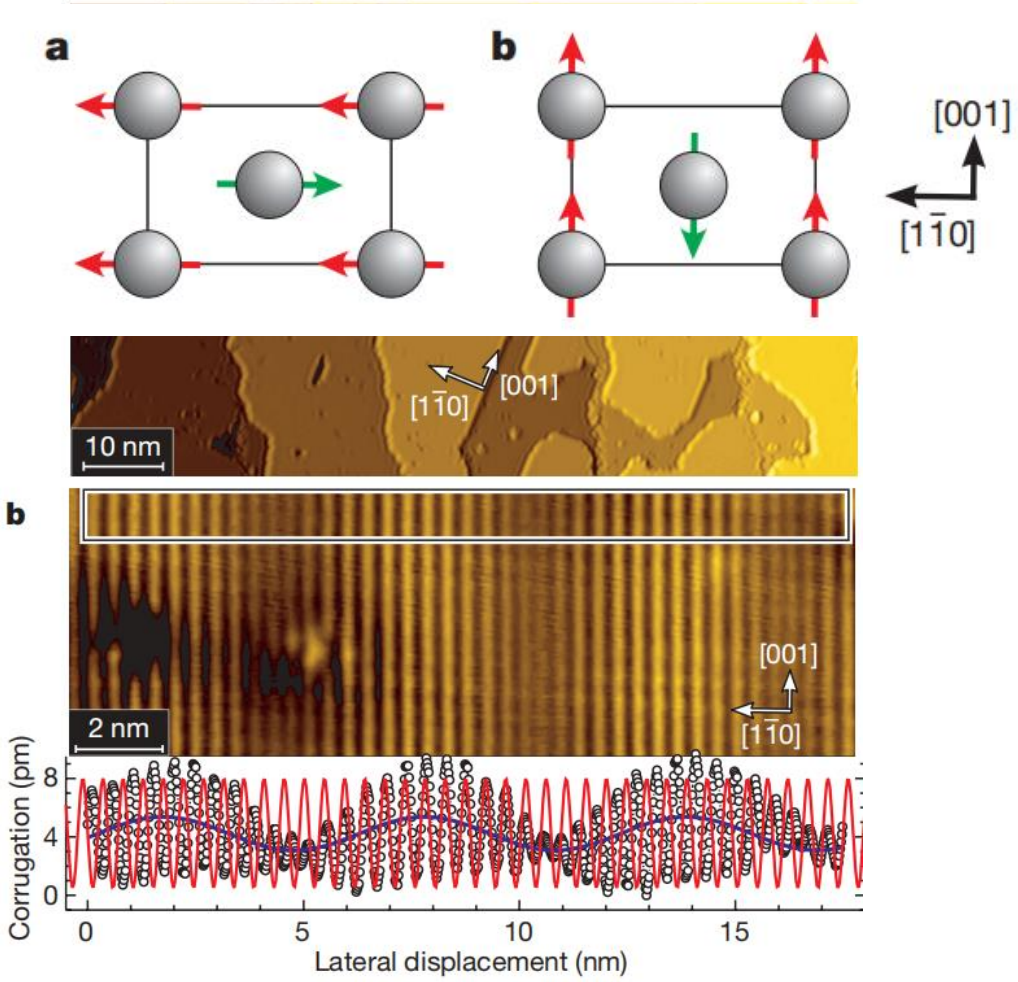

Bode, Matthias, et al.

Nature 447.7141 (2007): 190

Applications

Spin spiral states as an example of noncollinear spin structure

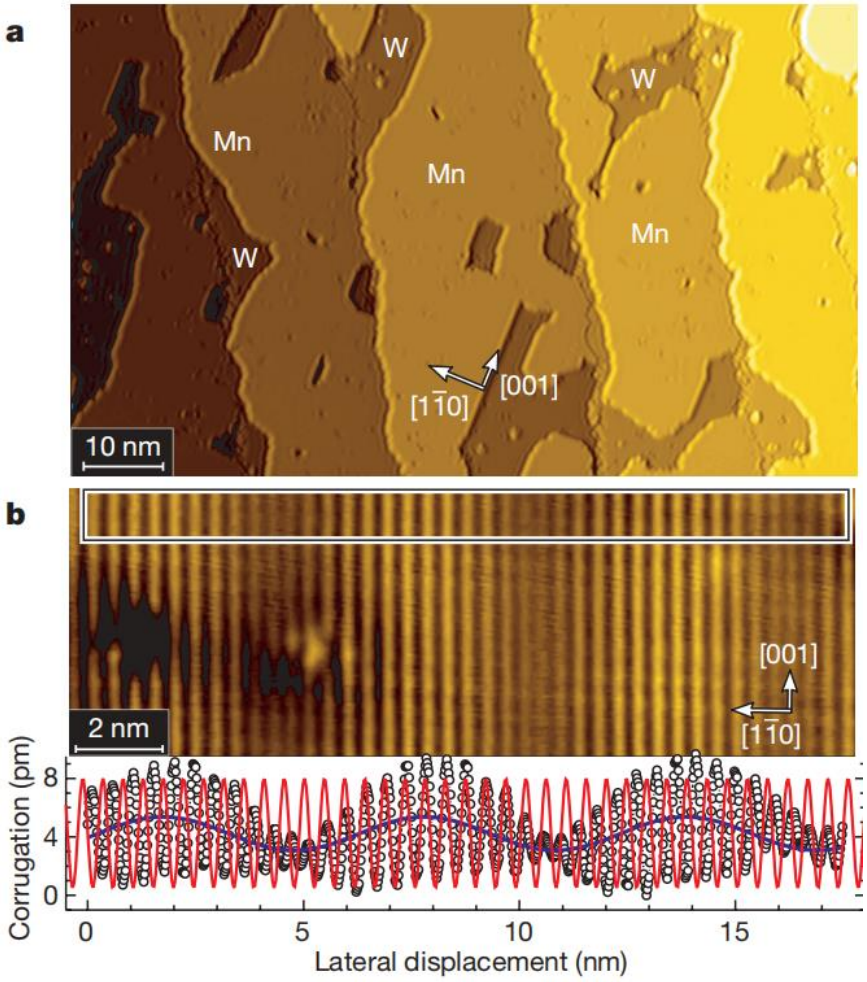

- an additional long wave modulation caused by the Dzyaloshinskii–Moriya interaction
- The long-wavelength modulation observed in Fig. b may be explained by two different spin structures:(1) a spin-density wave or(2) a spin spiral.

Bode, Matthias, et al.

Nature 447.7141 (2007): 190

Applications

Spin spiral states as an example of noncollinear spin structure

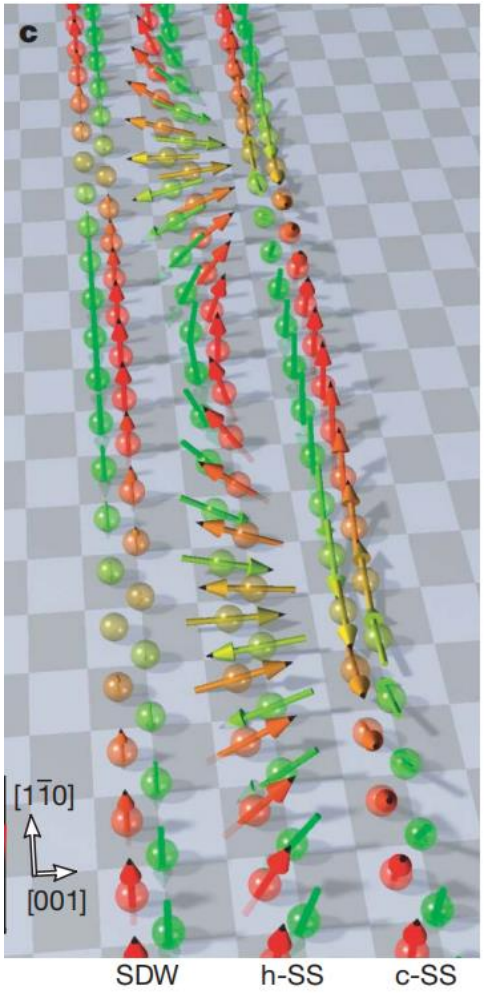

The magnetic contrast vanishes in either case twice over one magnetic period because
(1) the sample magnetic moments themselves vanish periodically or (2) the magnetic moments underneath the tip apex are orthogonal with respect to the tip magnetization, $\mathbf{m}_T$.

Bode, Matthias, et al.
Nature 447.7141 (2007): 190

Applications

Spin spiral states as an example of noncollinear spin structure

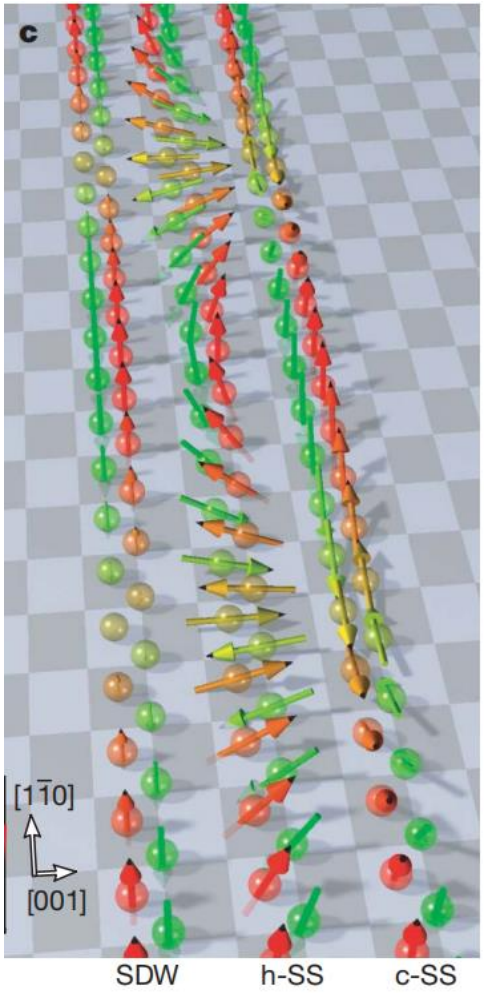

However, a distinguishment can be made because
in case (1) maximum spin contrast is always achieved at lateral positions where the magnetic moments are largest, independent of $\mathbf{m}_T$,
in case (2) a rotation of $\mathbf{m}_T$ can shift the position of maximum spin contrast.

Bode, Matthias, et al.
Nature 447.7141 (2007): 190

Applications

Spin spiral states as an example of noncollinear spin structure

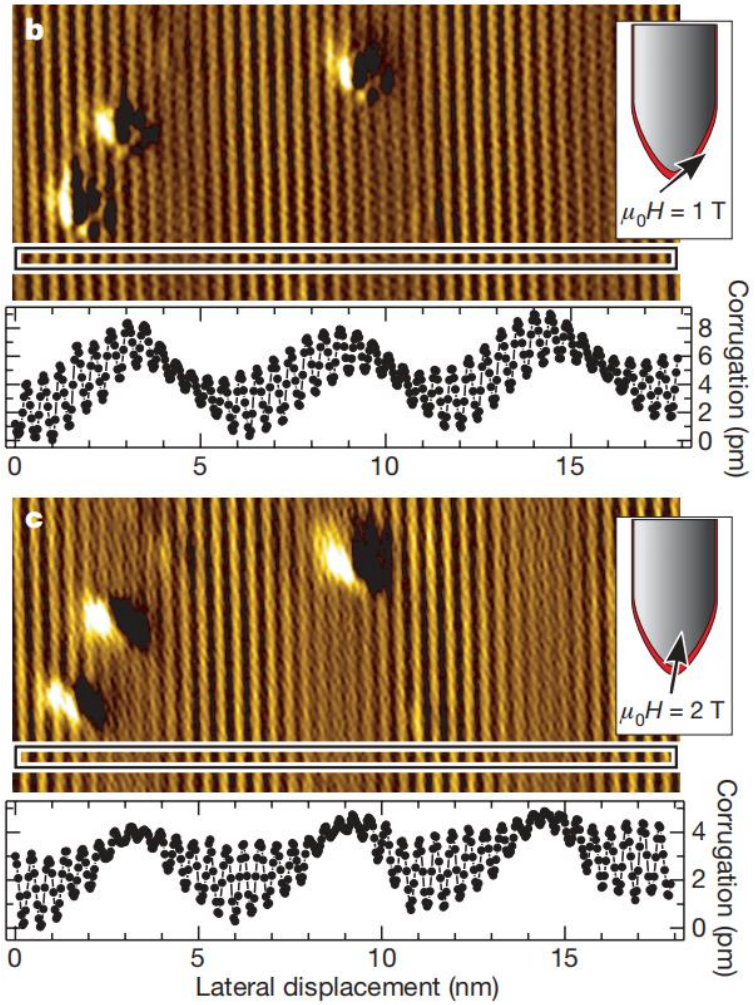

With increasing external field, the position of high magnetic corrugation shifts to the left.

This observation rules out a spin-density wave, but is a clear proof of a spin spiral with magnetic moments.

Bode, Matthias, et al.
Nature 447.7141 (2007): 190

谢 谢

Thanks